Chemosphere 254 (2020) 126842

Contents lists available at ScienceDirect

Chemosphere

journal homepage: www.elsevier.com/locate/chemosphere

Bioenhanced back diffusion and population dynamics of *Dehalococcoides mccartyi* strains in heterogeneous porous media

Jason P. Hnatko [a], Lurong Yang [a], Kurt D. Pennell [b], Linda M. Abriola [a], Natalie L. Cápiro [a, c, *]

[a] Department of Civil and Environmental Engineering, Tufts University, Medford, MA, USA
[b] School of Engineering, Brown University, Providence, RI, USA
[c] Department of Civil Engineering, Environmental Engineering Program, Auburn University, Auburn, AL, USA

HIGHLIGHTS

- Organohalide respiring bacteria enhanced mass transfer from low-permeability regions.
- Numerical models quantified bio-enhancement of back diffusion up to 53%.
- Bioenhancement was most pronounced near materials of contrasting permeability.
- *Dehalococcoides* cells were able to penetrate low-permeability media, including clays.
- *Dehalococcoides* strain distribution was influenced by available electron acceptor.

GRAPHICAL ABSTRACT

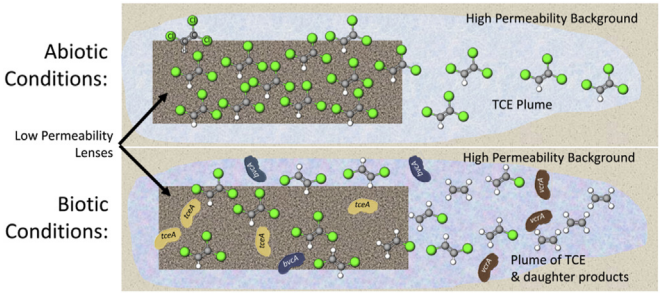

ARTICLE INFO

Article history:
Received 22 January 2020
Received in revised form
16 April 2020
Accepted 18 April 2020
Available online 22 April 2020

Handling Editor: Yongmei Li

Keywords:
Dehalococcoides mccartyi
Back diffusion
Trichloroethene
Bioenhanced mass transfer
Bioremediation
Low-permeability media

ABSTRACT

Diffusion, sorption-desorption, and biodegradation influence chlorinated solvent storage in, and release (mass flux) from, low-permeability media. Although bioenhanced dissolution of non-aqueous phase liquids has been well-documented, less attention has been directed towards biologically-mediated enhanced diffusion from low-permeability media. This process was investigated using a heterogeneous aquifer cell, packed with 20–30 mesh Ottawa sand and lenses of varying permeability (1.0×10^{-12}-1.2×10^{-11} m^2) and organic carbon (OC) content (<0.1%–2%), underlain by trichloroethene (TCE)-saturated clay. Initial contaminant loading was attained by flushing with 0.5 mM TCE. Total chlorinated ethenes removal by hydraulic flushing was then compared for abiotic and bioaugmented systems (KB-1® SIREM; Guelph, ON). A numerical model incorporating coupled diffusion and (de) sorption facilitated quantification of bio-enhanced TCE release from low-permeability lenses, which ranged from 6% to 53%. Although *Dehalococcoides mccartyi (Dhc)* 16S rRNA genes were uniformly distributed throughout the porous media, strain-specific distribution, as indicated by the reductive dehalogenase (RDase) genes *vcrA*, *bvcA*, and *tceA*, was influenced by physical and chemical heterogeneity. Cells harboring the *bvcA* gene comprised 44% of the total RDase genes in the lower clay layer and media surrounding high OC lenses, but only 2% of RDase genes at other locations. Conversely, cells harboring the *vcrA* gene comprised 50% of RDase genes in low-permeability media compared with 85% at other locations. These results demonstrate the influence of microbial processes on back diffusion, which was

* Corresponding author. 208 Harbert Center, Auburn University, Auburn, AL, 36849, USA.
E-mail address: natalie.capiro@auburn.edu (N.L. Cápiro).

https://doi.org/10.1016/j.chemosphere.2020.126842

most evident in regions with pronounced contrasts in permeability and OC content. Bioenhanced mass transfer and changes in the relative abundance of *Dhc* strains are likely to impact bioremediation performance in heterogeneous systems.

1. Introduction

Engineered bioremediation, including bioaugmentation and biostimulation, has been implemented as an effective remedial strategy to transform tetrachloroethene (PCE) and trichloroethene (TCE) to benign ethene, and has resulted in reduced site cleanup times compared to natural attenuation (e.g. Baldwin et al., 2017; Hood et al., 2008; Major et al., 2002). In close proximity to non-aqueous phase liquid (NAPL) contaminants, it is well documented that the process of microbial reductive dechlorination (MRD) can enhance organic phase dissolution rates over abiotic dissolution alone, leading to decreased longevity of the source zone (Amos et al., 2009; Cápiro et al., 2015; Sleep et al., 2006; Yang and McCarty, 2000). Two mechanisms involved in this enhancement are: (1) the transformation of contaminants to higher solubility daughter products, and (2) an increase in the concentration gradient between the NAPL and the surrounding aqueous phase (dissolution driving force).

While engineered bioremediation has been successfully implemented at many sites, numerous sites have also exhibited incomplete dechlorination to dichloroethene isomers (DCE) and/or vinyl chloride (VC) (Kielhorn et al., 2000; Lendvay et al., 2003; Major et al., 2002), or have demonstrated rebound of contaminant concentrations after biostimulation (McCarty, 2010; Tillotson and Borden, 2017). Contaminant rebound is often exacerbated by the presence of subsurface heterogeneity, where contaminant mass sequestered in low-permeability porous media can be slowly released over time through diffusion and desorption (McGuire et al., 2006; Sale et al., 2013; Simpkin and Norris, 2010; van Genuchten and Alves, 1982). Subsurface heterogeneity also complicates bioremediation because amendments delivered through groundwater injection are unable to effectively penetrate low-permeability media (Löffler et al., 2013; Sale et al., 2013; Simpkin and Norris, 2010). Despite these challenges, bioremediation has been shown to be effective in aquifers with physical heterogeneity, including clay tills (Damgaard et al., 2013a; Scheutz et al., 2010). Further, biological activity in higher permeability zones, where amendments are more easily distributed, can facilitate the back diffusion of compounds from low-permeability zones to higher flow regions by increasing the driving force for mass transfer (Chambon et al., 2010; Lima and Sleep, 2007; Scheutz et al., 2010).

The widespread application of MRD for treatment at chlorinated solvent sites has been largely due to the extensive study of *Dehalococcoides mccartyi* (*Dhc*) strains (Adrian et al., 2016; Grostern and Edwards, 2006; He et al., 2005, 2003; Löffler et al., 2013; Maymó-Gatell et al., 1999; Sung et al., 2006). This work has shown that numerous strains can contribute to the transformation of the PCE and TCE to benign ethene. Specific transformation steps are carried out by *Dhc* strains harboring reductive dehalogenase (RDase) genes, including *tceA*, (TCE to VC), *vcrA* (*cis*-DCE to ethene), and *bvcA* (all DCE isomers to ethene) (Löffler et al., 2013; Yoshikawa et al., 2017). RDase genes are routinely monitored to assess the dechlorination capability of specific microbial communities (Damgaard et al., 2013a; Lee et al., 2008; Ritalahti et al., 2006; Van Der Zaan et al., 2010).

While previous studies have examined responses of specific *Dhc* strains to perturbations in geochemistry (Amos et al., 2008; Yang et al., 2017; Marcet et al., 2018a), few have explored the influence of coupled physical and chemical heterogeneity on *Dhc* strain growth and activity despite the role of specific *Dhc* strains and the influence of subsurface conditions on the successful application of bioremediation. Instead, experimental studies have generally been limited to batch and one-dimensional homogeneous column experiments examining the relationship between electron donor and acceptor concentration and the abundance of RDase genes (Behrens et al., 2008; Doğan-Subaşi et al., 2014; Liang et al., 2015; Mirza et al., 2016). Such experimental systems, however, do not reproduce the heterogeneity present in real aquifers. Conversely, field-scale studies examining microbial population variations between sites or across large areas (Lee et al., 2008; Van Der Zaan et al., 2010; Yoshikawa et al., 2017) did not resolve microbial spatial distributions at the scale that will control enhanced contaminant mass transfer and its contribution to remedial effectiveness. Only one study examining the impacts of NAPL saturation heterogeneity on *Dhc* strain distribution has been performed in a heterogeneous multi-dimensional system (Cápiro et al., 2015), but the influence of physical heterogeneity was not addressed.

Mathematical models can be used to extrapolate laboratory results to the field-scale and to delineate the impact of individual biogeochemical processes. In prior studies, models have been used to quantify the effect of back diffusion in both field- and bench-scale systems (2-D) incorporating heterogeneous permeability domains (Chapman and Parker, 2005; Chapman et al., 2012; Parker et al., 2008; Rodriguez, 2006). However, these investigations have not accounted for coupled processes, including diffusion, sorption, and biotransformation. Changes in physical-chemical properties (e.g., diffusivity, solubility, sorptive capacity, volatility) as parent compounds are biotransformed to daughter products will also influence the remediation of the sequestered mass in low-permeability soils. To date, no studies have utilized numerical models to quantify the impact of enhanced biotransformation on back diffusion in heterogeneous media.

Due to the potential impacts of bioremediation on contaminant mass transfer from low-permeability zones, there is a critical need for systematic, high-resolution laboratory investigations of biomass and *Dhc* strain distributions in realistic, multi-dimensional, chemically and physically heterogeneous systems. The overall objective of this study was to improve our understanding of the contribution of bioremediation to mass transfer between the bulk media and regions of low-permeability and higher organic carbon (OC). A laboratory-scale multi-dimensional aquifer cell, packed with five porous media of varying permeability and OC content, was employed to study chlorinated ethene (TCE) diffusion from low-permeability regions under abiotic and biotic conditions. A modified version of a three-dimensional multi-species modular transport model (MT3DMS), incorporating information on physical and sorption heterogeneity, was used to generate predictions of back diffusion under abiotic conditions for comparison with experimental data following bioaugmentation. The spatial and temporal variation abundance of *Dhc* 16S rRNA and RDase genes was monitored throughout the experiment and in soil samples collected at the conclusion of the experiment. These data were used to

determine the extent of biologically-enhanced back diffusion as a function of physical heterogeneity, contaminant distribution, and the distribution of total and specific *Dhc* strain abundance.

2. Materials and methods

2.1. Aquifer cell setup and preparation

The aquifer cell (63.5 cm length × 38 cm height × 1.4 cm thickness) was constructed from two 1.4 cm thick glass panels held in an aluminum frame, with sampling ports aligned in four vertical columns following the procedures of Cápiro et al. (2015) and Suchomel et al. (2007) (Fig. 1). Clay collected from the Commerce Street Superfund Site (Williston, VT) was dried, ground with a mortar and pestle, re-saturated with a 100 mg/L TCE solution, and emplaced in the bottom 3 cm of the aquifer cell to create a lower confining layer. Above the clay layer, the aquifer cell was packed with ASTM International Standard 20–30 mesh sand (US Silica Company; Ottawa, IL) under water-saturated conditions. Four 5 cm (height) x 14 cm (length) lenses were emplaced so that sampling ports were located downgradient from each lens. Lens materials consisted of Webster soil (Iowa State University Agricultural Experiment Station; Ames, IA), Appling soil (University of Georgia Agricultural Experiment Station; Eastville, GA), F-95 sand (Fisher Scientific; Hampton, NH), and a loamy sand collected from the Commerce Street site (Fig. 1). All porous media was sterilized via autoclave, liquid cycle at 121 °C for 30 min, prior to packing. Additional porous media information can be found in Table 2 and the Supplementary Material (SM).

After packing, flow was established in the aquifer cell using a constant head influent system described by Cápiro et al. (2015). Influent solutions were prepared in a 5 L Mariotte bottle, and a flow rate of 0.10 (during biotic treatment) to 2.60 (during bromide tracer test) mL/min was maintained by adjusting the height of the influent and effluent reservoirs (Table 1). These flow rates correspond to seepage (pore-water) velocities of 7.47–82.5 cm/day and residence times of 0.77–8.5 days.

2.2. Non-reactive tracer and abiotic back diffusion experiments

A conservative tracer test was performed using a 10 mM sodium bromide (Fisher Scientific; Hampton, NH) and 0.075 mM sodium fluorescein (Sigma Aldrich; St. Louis, MO) solution as described in the SM. The abiotic back diffusion experiment was completed in two phases that are detailed in Table 1. Briefly, after the tracer test, an influent solution of 0.5 mM TCE and 10 mM sodium bromide was maintained for 15.9 pore volumes (PVs) to simulate historic mass loading (plume development). This duration was based on model predictions estimating a minimum of 15 PVs to allow bromide and TCE to fully penetrate low permeability materials. Following the loading stage, the influent was changed to a 10 mM sodium chloride solution (without TCE) to flush TCE and bromide from the aquifer cell. During this abiotic flushing period, 1.6 mL samples were collected periodically from 12 sampling ports using a Fusion 200 syringe pump (Chemyx; Stafford, TX) to draw samples at a rate of 0.1 mL/min (10% of the background flow rate). Effluent samples (1.6 mL) were also collected from a 20 mL sampling bulb in the effluent line. Sample aliquots (1.0 mL) were used to measure chlorinated ethenes (TCE, *cis*-DCE, and VC) and ethene concentrations using a gas chromatograph equipped with a flame-ionization detector (GC-FID) and the remaining sample volume (0.6 mL) was analyzed for bromide concentrations by ion chromatography. Details of the analytical methods are provided in the SM. The 12 sampling port locations were selected based upon their locations relative to the clay and soil lenses and to provide a sampling port downgradient of each lens.

2.3. Biotic degradation experiment

Following the abiotic back diffusion experiment, the cell was again pre-loaded with TCE over a 22.6 PV injection period. To achieve conditions appropriate for MRD, TCE loading was conducted in three phases (Table 1). After an initial preloading using a 0.5 mM TCE influent solution (TCE Plume Development I), anoxic conditions were established by introducing a bacterial growth

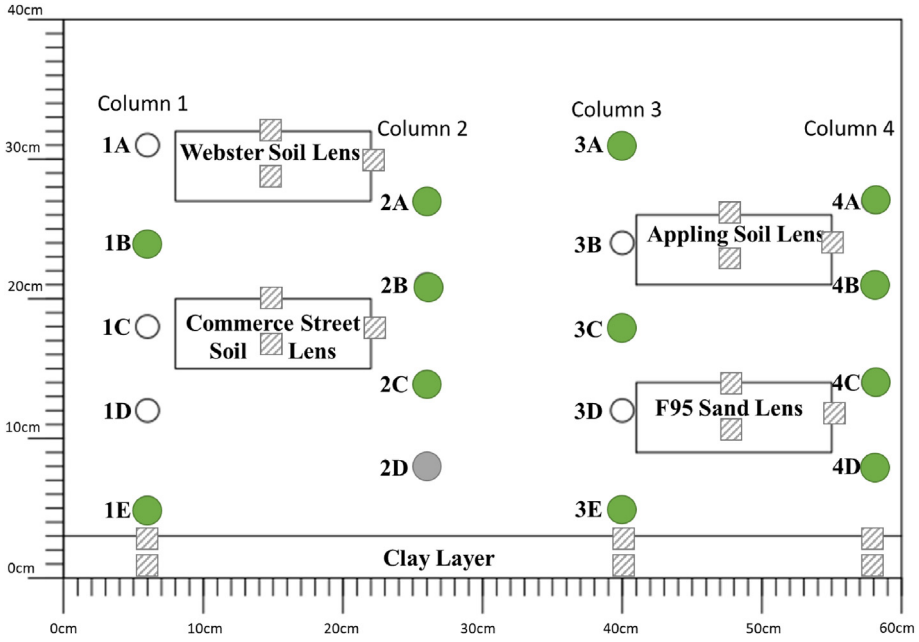

Fig. 1. Aquifer cell layout and sample locations. Solid green circles represent aqueous sampling ports sampled throughout experiment, a solid gray circles represents a port samplid during the final 7 rounds only, and hatched squares represent additional soil sample locations.

Table 1
Aquifer cell experimental parameters.

Phase	Bromide Tracer		Bromide Flushing	Abiotic Experiment		
	Bromide Plume Development			Bromide/TCE Plume Development		Abiotic Flushing
Avg. Flow Rate (mL/min)	2.4		2.4	1.0		0.93
Duration (PVs)	0.63		2.3	15.9		8.9
Duration (days)	0.21		0.79	13		8
Influent Solution	10 mM sodium bromide and 0.075 mM sodium fluorescein		10 mM sodium chloride	10 mM sodium bromide		10 mM sodium chloride
Influent TCE	0 mM		0 mM	0.5 mM		0.01 mM
Sampling Frequency	1/0.04 PVs (effluent only)			1/0.06 to 1/3.9 PVs (effluent and ports)		
	Biotic Experiment					
Phase	**TCE Plume Develop-ment I**	**TCE Plume Develop-ment II**	**TCE Plume Develop-ment III**	BIOAUGMENTATION	**Establish Microbial Community**	**Biotic Treatment I**	**Biotic Treatment II**
Avg. Flow Rate (mL/min)	0.51	0.71	0.39		0.27	0.21	0.16
Duration (PVs)	12.9	6	3.7		2.6	5.8	1.5
Duration (days)	21	7	8		8	23	8
Influent Solution	10 mM sodium chloride	Mineral Salts Medium with 10 mM sodium lactate			Mineral Salts Medium with 10 mM sodium lactate		
Influent TCE	0.5 mM	0.5 mM	0.5 mM		0.5 mM	0.04 mM	0.01 mM
Sampling Frequency	1/0.23 to 1/1.2 PVs (effluent and ports)						

medium, augmented with 10 mM sodium lactate and 0.5 mM TCE, as the influent (TCE Plume Development II). The medium was prepared according to Löffler et al. (2005), incorporating the modifications reported in Cápiro et al. (2015). Prior to bioaugmentation (TCE Plume Development III), the flow rate was reduced to approximately 0.39 mL/min (34 cm/day seepage velocity; 1.8-day residence time) to provide sufficient residence time for biodegradation reactions to occur. The aquifer cell was then bioaugmented with the KB-1® inoculum (SiREM; Guelph, Ontario), a methanogenic dechlorinating consortium containing *Acetobacterium* sp., *Geobacter* sp. *(Geo),* and multiple *Dhc* strains harboring the *vcrA, bvcA, and tceA* RDase genes. This consortium was selected based upon its widespread application in the field, previous use in field-scale bioremediation applications, and demonstrated capability to dechlorinate PCE to ethene (Duhamel et al., 2004, 2002; Sleep et al., 2006). Initial gene abundances of 2.4×10^7, 9.8×10^7, 2.9×10^6, and 6.0×10^5 gene copies/mL of the *Dhc* 16S rRNA, *vcrA*, *bvcA*, and *tceA* genes, respectively, were measured in the inoculating culture. The inoculum was diluted in sterile growth medium to provide approximately 10^4 *Dhc* cells/mL of pore water, the cell density suggested by previous studies to yield ethene at acceptable rates (Adrian et al., 2016; Clark et al., 2018). Twenty mL of dilute inoculum was then injected at a rate of 0.1 mL/min into each of the 18 sampling ports using a syringe pump in an effort to create a uniform distribution.

Following bioaugmentation, influent consisting of medium, lactate, and TCE was maintained for 2.6 PVs to establish the microbial community. The influent TCE concentration was then reduced to 0.04 mM for 5.8 PVs (Biotic Treatment I) and to 0.01 mM for 1.5 PVs (Biotic Treatment II) as shown in Table 1. Samples (1.0–2.6 mL) were collected from selected sampling ports and from the effluent throughout the experiment. These samples were analyzed for chlorinated ethenes and ethene by GC-FID as described above, with additional 0.5 mL aliquots analyzed for volatile fatty acids (VFAs) by high pressure liquid chromatography (HPLC). The remaining sample volume was centrifuged and frozen for microbial quantification via quantitative polymerase chain reaction (qPCR) as described in the SM (Cápiro et al., 2015; Ritalahti et al., 2006). An additional port (2D, Fig. 1), located near the clay layer, was sampled once ethene was the only compound detected in the effluent (6.6 PVs after bioaugmentation) to monitor diffusion from the clay. Following the final round of aqueous port sampling, the aquifer cell was destructively sampled to measure sorbed-phase chlorinated ethenes and attached biomass at specific locations (at the sampling port locations, in the clay confining layer, and within and around each lens, see SM for details).

2.4. Numerical simulation

A modified version of MT3DMS (Yang et al., 2018) was used to simulate bromide tracer and abiotic TCE back diffusion experiments, and to quantify bioenhanced chlorinated ethenes and ethene diffusion. This model was coupled with MODFLOW (McDonald and Harbaugh, 1988) to simulate transient flow conditions. In MT3DMS, aqueous transport of non-reactive components is represented by a traditional advection-dispersion-reaction equation (SM-1.5 equation (1)). In this work, TCE sorption to solids was represented as a linear, equilibrium process (SM-1.5 equation (2)).

Initial model parameter values (Table 2) were obtained from published experiments conducted with the same porous media. Data from the bromide tracer experiment were used to characterize the flow field and fit hydraulic parameters (hydraulic conductivity and dispersivity coefficients) in the numerical model.

Table 2
Initial and calibrated model parameters for aquifer cell transport simulations.

Porous Media	Published Values			Model Calibrated Values		Measured[a]
	Organic Carbon Content (% mass)	Hydraulic Conductivity (m/day)	Linear Sorption Coefficient, K_d(L/kg)	Hydraulic Conductivity (m/day)	Linear Sorption Coefficient, K_d(L/kg)	Porosity, φ (−)
ASTM 20/30	N/A	330[b]	N/A	200	0	0.45
Webster Soil	1.96%[c]	0.86[d]	2.47[e]	0.6	4.16	0.51
Appling Soil	0.66%[c]	10.2[f]	0.83[e]	5	0.95	0.33
Commerce St. Soil	0.09%[g]	1.7–6.9[g]	0.13[g]	5	0.13	0.3
F-95 Sand	0.01%[c]	1.9[h]	0.006[i]	1	0.0013	0.28
Commerce St. Clay	0.30%[g]	N/A[j]	0.35[g]	0.05	0.40	0.78

[a] Measured in this experiment by mass added and aquifer cell volume.
[b] Taylor et al.(2001).
[c] Marcet et al.(2018b).
[d] Marcet(2014).
[e] Calculated by $K_d = Orgranic\ Carbon\ Content{*}K_{OC}$ using the organic carbon content from Marcet et al. (2018b) and $K_{OC} = 126\ L/kg$for TCE from Pankow et al. (1996).
[f] Pennell et al.(1995).
[g] Gaeth (2017).
[h] Chen et al.(2007).
[i] Joo et al.(2008).
[j] N/A = not available

Details of breakthrough curve fitting are provided in Section SM-2.1. A comparison of simulated and measured TCE (sorptive) and bromide (conservative) concentrations at sampling ports and in the effluent during the abiotic flushing experiment facilitated calibration of the linear sorption coefficients (K_d). Porosity was calculated from experimental measurements of soil mass and emplaced volume. Free-solution diffusivity values for bromide and TCE were 2.01×10^{-5} cm^2/s and 7.99×10^{-6} cm^2/s, respectively (Li and Gregory, 1974; Verschueren, 2001). A tortuosity of 0.67 (Ball et al., 1997; Johnson et al., 1989) was used to obtain the effective diffusivity used in the model following the method by Yang et al. (2018).

The total molar sum of chlorinated ethenes and ethene concentrations (total ethenes) observed during the biotic experiment were compared with model predictions of concentrations expected in the absence of MRD to assess the influence of biotransformation on diffusion and desorption (bioenhancement of back diffusion). Detailed descriptions of model simulation procedure, domain discretization, and boundary conditions are provided in Section SM-1.5.

3. Results and discussion

3.1. Desorption and diffusion under abiotic conditions

Measurements from the abiotic flushing experiment were used in conjunction with model simulations to investigate the influence of sorption and diffusion on the removal of sorbing (i.e., TCE) and non-sorbing (i.e., bromide) solutes (Fig. 2). One PV after reducing the solute influent concentrations, the concentrations dropped rapidly, with the effluent TCE and bromide concentrations reduced to 16.9% and 8.5% of the loading concentrations, respectively. After 9 PVs of flushing, TCE concentrations were one order-of-magnitude lower than the input concentration, while bromide concentrations were two orders-of-magnitude lower than the input concentration. Based on model simulations, the TCE mass retention percentages from each porous material at the final flushing time were 2.7%, 51.5%, 26.4%, 2.6%, 4.1%, and 20.1% in the background sand, Webster lens, Appling lens, Commerce Street lens, F-95 sand lens, and clay layer, respectively. This higher retention of TCE in comparison to that of bromide (which had 1.9% mass retention in the clay layer and 0.3% in other locations) is attributed primarily to the influence of sorption.

Measurements and model predictions of bromide and TCE concentrations during the abiotic flushing period are presented in Fig. 2 for the effluent, a port above the clay layer [1E], a port downgradient of the Commerce Street lens [2C], and a port downgradient of the F95 sand lens [4D]. These locations were selected based upon their proximity to low-permeability materials that can retain contaminant mass and thus, support back diffusion and desorption. The agreement between model predictions and experimental measurements indicates that the model is capable of capturing measured bromide and TCE back diffusion under abiotic conditions, with goodness of fits of 0.91 and 0.95 in the effluent, 0.88 and 0.91 at port 1E, 0.99 and 0.86 at port 2C, and 0.98 and 0.84 at port 4D for bromide and TCE, respectively. Although the geometry of the low-permeability compartments was digitized based on images of the aquifer cell, fine-scale variations in lens shape and compaction of the material may partially account for the discrepancies between model simulations and experimental measurements.

3.2. Biodegradation results

The biotic experiment utilized a TCE loading approach similar to that employed during the abiotic experiment. Following bioaugmentation, *cis*-DCE was detected in the effluent after 0.2 PVs (5% of the total ethenes), VC was detected after 2 PVs (1% of total ethenes), and ethene after 3.4 PVs (4% of total ethenes). When the influent TCE concentration was lowered to 0.04 mM, 2.6 PVs after bioaugmentation, the effluent molar composition was 90% *cis*-DCE and 10% VC (Figure SM-5[a]). Approximately 6.1 PVs after bioaugmentation, 3.4 PVs after lowering the influent TCE concentration to 0.04 mM, ethene was the only analyte detected in the effluent. However, *cis*-DCE continued to be detected at concentrations of 0.07–0.08 mM in sampling ports located near the influent chamber (1A and 1E, Fig. 1) and at 0.02–0.03 mM in the ports located in columns 2 and 3 (Fig. 1), indicating rapid biotransformation of TCE to *cis*-DCE and slower transformation to VC and ethene.

When the influent TCE concentration was further reduced to 0.01 mM (9 PVs after bioaugmentation), ethene persisted in the effluent at 0.04–0.06 mM, indicating additional mass inputs from diffusion and desorption from the low-permeability lenses and clay. Ethene concentrations were sustained at 0.01–0.02 mM in all ports except those impacted by the clay (1E and 3E) and the higher OC lenses (3A, 4A, and 4B) where higher ethene concentrations were measured (Figure SM-5). The highest concentrations, 0.04–0.06 mM, were measured in the bottom ports (1E and 3E),

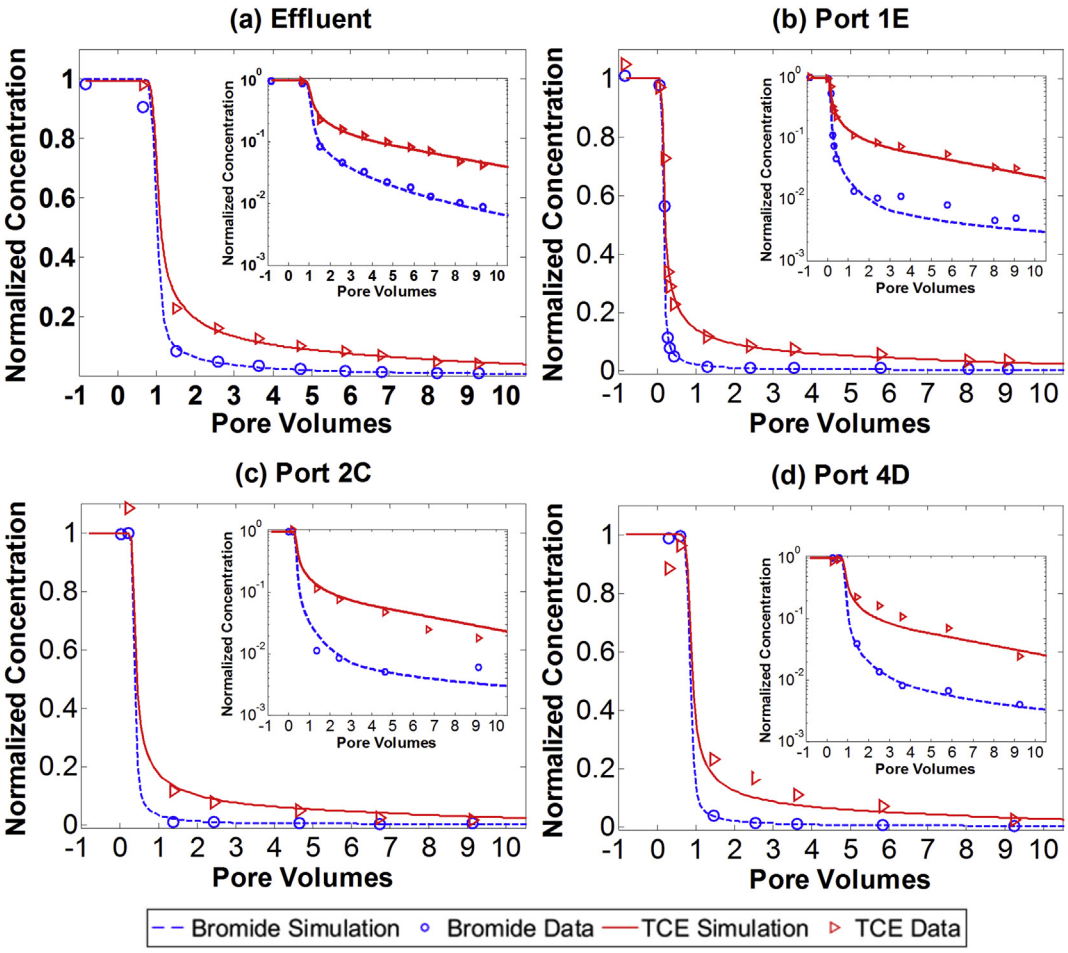

Fig. 2. Comparison of experiment observations and calibrated model simulations of bromide and TCE concentrations (normalized by input concentration) plotted in linear and log scale (inset) during abiotic flushing experiment in (a) effluent (b) port 1E (c) port 2C and (d) port 4D. Influent TCE and bromide concentrations were switched to 0.01 and 0.0 mM at time zero (PV = 0), respectively Experiment data: circle—bromide, triangle—TCE; Simulation: dashed line—bromide, solid line—TCE.

where TCE continued to be released from the underlying clay layer (Figure SM-5 [b] and [d]). Downgradient of the high OC Webster and Appling lenses (ports 3A, 4A, and 4B), ethene was detected at concentrations up to 0.03 mM.

At the conclusion of the experiment, TCE was detected in soil samples collected from the clay layer, Webster lens, and Appling lens with average concentrations of 1.94 μg/g (±0.57 μg/g), 0.022 μg/g (±0.016 μg/g), and 0.37 μg/g (±0.19 μg/g), respectively. Due to the high detection limit for *cis*-DCE (0.0026 mM) as described in the SI, this compound was only detected in the clay layer at an average concentration of 49 μg/g (±23 μg/g). Throughout the experiment, lactate, acetate, and/or propionate were detected in all samples indicating excess electron donor. Total VFA concentrations in sampling ports and effluent averaged 3.69 mM (±1.71 mM) and 2.37 mM (±0.21 mM), respectively.

3.3. Desorption and diffusion under abiotic and biotic conditions

To explore the influence of MRD on chlorinated ethene mass transfer, a synthetic abiotic flushing experiment (with the same influent conditions but without MRD) was created by numerical simulation and model predictions were compared with measurements of total ethenes during the biotic experiment. Under biotic conditions, TCE transformed to the lesser-chlorinated transformation products, which have higher diffusivities, higher solubilities, and lower sorption coefficients than TCE. This transformation increases the mobility of the compounds, thus increasing the driving force for back diffusion, resulting in microbially-enhanced mass transfer. As the comparative simulation used the same flow rate and input concentration of TCE as the MRD experiment, comparison of aqueous mass (measured biotic vs. modeled abiotic) at sampling locations indicates the influence of MRD on contaminant mass transfer. An expression to quantify the extent of bioenhanced back diffusion and desorption was developed as:

$$\delta_{MRD} = \frac{CM_{exp} - CM_{sim}}{CM_{sim}} \times 100\% \quad (1)$$

Here, δ_{MRD} is a measure of the effective enhancement of TCE diffusion and desorption by MRD, CM_{exp} is the total ethene molar mass calculated using experimental data for a specific location (e.g., effluent or sampling port), and CM_{sim} is the TCE molar mass calculated using the model simulation at the same location. CM_{exp} or CM_{sim} is calculated by a stepwise summation of the discrete data of total concentration, $\sum_{i_t=0}^{i_{t=final}} (total\ concentration)_{i_t} \times (time\ interval)_{i_t} \times (flow\ rate)_{i_t}$. Predicted and measured concentrations of total ethenes in the effluent and selected ports are compared in Fig. 3 with subplots for the two ports with the highest δ_{MRD} values, both located at the bottom of the aquifer cell (near the clay layer).

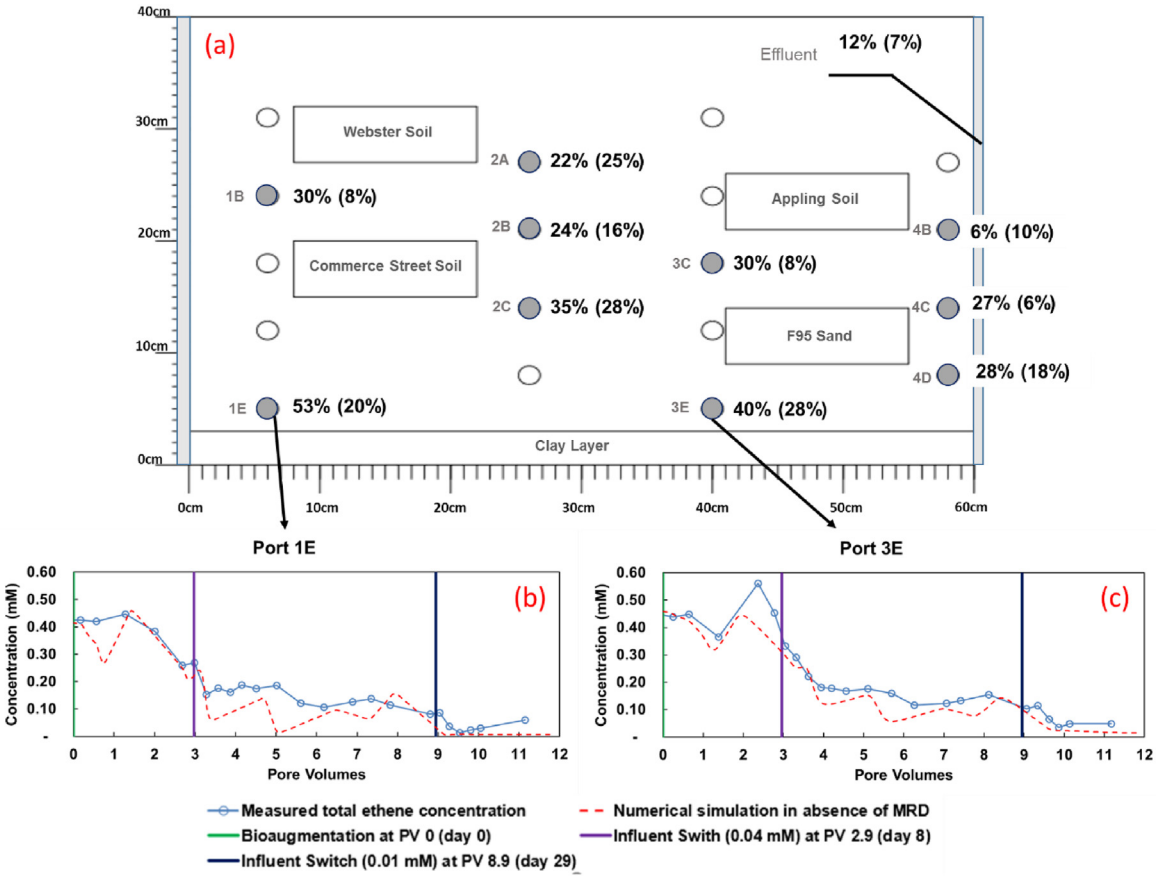

Fig. 3. Bioenhancement of back diffusion and desorption in the heterogeneous aquifer cell; (a) δ_{MRD} (%) in effluent and selected ports where percentage values were calculated for the period from the lowering of the influent TCE concentration (PV 2.9) to the end of the experiment, and over the period of the entire biotic experiment (shown in parentheses), (b) and (c) show the total molar concentration of chlorinated ethenes and ethene during biotic experiment compared with model simulations without MRD for port 1E and 3E, respectively.

The δ_{MRD} values (Fig. 3) reveal that total ethenes mass elution was enhanced by MRD, with $\delta_{MRD}>0$ calculated at all sampling locations (12% for the effluent and 6%–53% at the sampling ports). Sampling ports directly impacted by mass transfer from low-permeability layers displayed more pronounced differences from abiotic simulations than ports located downgradient of more permeable materials. For example, ports 1E and 3E, in close proximity to the clay layer (lowest permeability and higher sorption capacity than background sand), displayed the highest MRD enhancements of 53% and 40%, respectively. Similar enhancements were observed in other locations near low-permeability zones (Figure SM-6). The ports immediately downgradient from the Webster (port 2A), Commerce Street (port 2B and 2C), and F-95 soil lenses (port 4C and 4D) were associated with bioenhanced mass transfer ranging from 22% to 35%. Lower enhancement (12%) was measured in the effluent, attributed to dilution from the more permeable, less sorptive zones. However, the lowest δ_{MRD} was measured at port 4B, immediately downgradient from the Appling soil lens, which has a higher organic carbon content than the Commerce Street and F95 lenses. This observation may be attributed to volatilization losses; TCE biodegradation products (*cis*-DCE, VC, and ethene) have higher volatility than TCE and the location of this port is nearest to air-water contact surface of the aquifer cell. Thus, the volatilization losses from the water table in the vicinity of port 4B may have resulted in a reduction in measured chlorinated ethene mass, and an underestimation of total δ_{MRD}. As the effluent represents the integrated effect of all locations in the aquifer cell, the δ_{MRD} calculated for the effluent may also be underestimated due to volatilization.

3.4. Growth of Dehalococcoides population

Total *Dhc* abundance, as measured by the 16S rRNA gene, increased from a 12-port average of $2.8 \times 10^5 \pm 4.4 \times 10^5$ cells/mL following bioaugmentation (0.5–0.9 PVs) to $3.8 \times 10^7 \pm 1.5 \times 10^7$ cells/mL at the conclusion of the experiment (Figure SM-7, Table SM-1). At an intermediate sampling time, 5.2 PVs after bioaugmentation, *Dhc* abundance varied 3 orders-of-magnitude across the domain, with the highest abundance in downgradient ports (columns 3 and 4, average abundance $7.1 \times 10^7 \pm 4.6 \times 10^7$ cells/mL), where higher concentrations of *cis*-DCE and VC were present, and the lowest in the upgradient ports (columns 1 and 2, average abundance $9.6 \times 10^6 \pm 6.1 \times 10^6$ cells/mL). This observation may be explained by the fact that *Geo* cells are more efficient than *Dhc* cells at transforming TCE to *cis*-DCE and can outcompete *Dhc* when TCE is present (i.e., at upgradient ports) (Amos et al., 2009; Duhamel and Edwards, 2007). *Dhc* abundance was higher where *cis*-DCE and VC were the available electron acceptors (i.e., downgradient ports, Figure SM-7). The uniform *Dhc* population at the conclusion of the experiment, when all measurements were within one order-of-magnitude, may reflect electron acceptor limitations and an associated lack of competition by *Geo* in the last phase of the experiment (lowest TCE influent). During the period of higher TCE influent concentration (2.6 PVs), *Geobacter lovely strain SZ (GeoSZ)* abundance, as measured by qPCR of the 16S rRNA gene, increased from an initial value of

8.0×10^1 cells/mL to an average of $2.2 \times 10^6 \pm 2.3 \times 10^6$ cells/mL, but growth ceased after influent TCE was lowered (Table SM-1).

In solid phase samples collected at the conclusion of the experiment, total *Dhc* abundance was uniform in the background samples (collected from sand corresponding to the sampling port locations), averaging $6.6 \times 10^7 \pm 1.4 \times 10^8$ cells/mass of porous media containing 1 mL of water. Within the lenses, *Dhc* abundance was approximately two to four times higher throughout the Appling and Webster lenses, but four to six times lower in the Commerce Street and F-95 sand lenses. In samples collected from the clay layer, *Dhc* abundance was more than one order-of-magnitude lower than in the background (Table SM-1). Growth of *Dhc* cells in and around low permeability materials was responsible for the measured bioenhancement of back diffusion. Although aqueous samples were not collected from the clay layer and lenses to quantify chlorinated ethene transformation within these materials, the increase in *Dhc* abundance and detection of *cis*-DCE in the clay suggests active MRD. MRD in the clay layer, and/or at the interface between the clay and background materials, was supported by either the diffusion of supplied VFAs into the clay or components of the clay that could be used as an electron donor, leading to the highest δ_{MRD} (53% and 40%) measured in Ports 1E and 3E, directly above the clay (Fig. 3(a)).

At sampling port locations, cell abundances measured in co-located aqueous and sand samples were used to estimate the number of cells attached to the solid phase by subtracting the planktonic cells from the total cells (combined planktonic and solid phase associated cells) in the wet porous media at the same location. All measurements of gene copies in porous media were normalized by moisture content and porosity, and reported as the mass of porous media that would contain 1 mL of pore water when saturated, as in Amos et al. (2009). In all but 3 locations, 77%–100% of the cells were found to be associated with the aqueous phase. This condition is typical of cells lacking necessary growth substrates, and is consistent with the depleted electron acceptor (chlorinated ethenes) conditions after lowering the TCE influent to 0.01 mM (Cápiro et al., 2014). Although the ratio of attached and unattached cells could not be calculated during active MRD, previous studies suggest active dechlorination was carried out by attached cells (Amos et al., 2009; Cápiro et al., 2014; Chen et al., 2013; Schaefer et al., 2010). Although microbial transport is possible, its impact was minimized by inoculating the aquifer cell through all ports. Cápiro et al. (2014) reported that *Dhc* strains grow as attached cells in systems where substrates are available. Similarly, in this study, the growth of populations of cells harboring specific RDase occurred in locations where substrates were available, likely as attached cells. Downgradient from the Webster and Appling lenses (port 4B), which continued to release electron acceptor through diffusion and desorption, 53% of the *Dhc* 16S rRNA gene copies measured were associated with the solid phase. Near the influent (ports 1B and 1E), where TCE had been introduced throughout the experiment, most of the cells (90% and 74%, respectively) were attached to the solid phase, as sufficient electron acceptor was available.

3.5. Distribution of RDase genes

Immediately after bioaugmentation, the *tceA* gene was most abundant in the first column of ports, near the 0.5 mM TCE influent, comprising 43%–99% of the total RDase genes (Figure SM-8). After 2.6 PVs (Fig. 4), the *tceA* gene continued to be predominate (65%–85% of total RDase genes) in ports 3A and 4C, where a measurable concentration of VC had not been detected. At later times (5.2 PVs and 9.8 PVs after bioaugmentation, Fig. 4 and SM-7), cells harboring the *tceA* gene only comprised a substantial proportion of the total RDase genes (more than 30%) near the influent (port 1B), downgradient of the Commerce Street lens (port 2C), and above the clay layer (ports 1E and 2D). These are locations where TCE was introduced or stored in low-permeability, high-sorption regions. At the conclusion of the experiment, *tceA* was the only RDase gene detected in the clay sample collected 5 cm below Port 1E, where highest TCE [2.7 μg/g] and *cis*-DCE [95 μg/g] concentrations were measured. The *tceA* gene was also detected in the center of the Webster, Commerce Street, and F-95 lenses, accounting for 15%, 19%, and 45% of the total RDase genes, respectively. Cells harboring the *tceA* gene were associated with the solid phase (31%–100% attached) in all port locations but four, indicating that cells harboring the *tceA* gene may be able to remain attached even when lacking a growth substrate. In ports 1B, 2C, 4C, and 4D, only 0%–7% of the *tceA* genes measured were associated with the solid phase. Although *Dhc* cells were present, these locations were not impacted by the clay or high OC lenses; chlorinated ethenes were flushed rapidly from these regions, as reflected in the lowest ethene concentrations measured at the conclusion of the experiment. As cells in these locations faced the greatest electron acceptor limitation, fewer remained attached to the solid phase at the conclusion of the experiment.

In sampling ports located in columns 3 and 4 (further downgradient), where *cis*-DCE and VC were detected due to upgradient transformation of TCE, cells harboring the *vcrA* gene were more abundant than other *Dhc* cells in samples collected 0.6 and 2.6 PVs after bioaugmentation, comprising 62%–99% and 70%–85% of the RDase genes detected, respectively. By the end of the experiment, 81%–92% of the RDase genes detected in the aqueous phase were *vcrA* in all but 2 ports (1E, and 2D, both above the TCE-containing clay and in the upgradient half of the aquifer cell). Similarly, nearly all of the *Dhc* cells in the background porous media harbored the *vcrA* gene (75%–100%) in solid phase samples collected at the conclusion of the experiment, except where TCE continued to diffuse from the Commerce Street lens (port 2B) and clay layer (port 2E), as shown on Fig. 5. As with the *Dhc* 16S rRNA gene abundance, nearly all (93%–100%) of the *vcrA* genes measured at port sample locations were associated with the aqueous phase samples with a few exceptions. In ports 1B, 1E, and 4B, 45%–87% of the *vcrA* genes detected were associated with the solid phase, likely due to the accessibility of electron acceptor near the influent and downgradient of the high-OC Webster soil lens.

Cells harboring the *bvcA* gene made up a small proportion of the population (0%–9%) at early time (0.6 PVs), except where the total RDase gene abundance was lowest (Port 2B, 28%, and Port 3C, 18%). Subsequently (PVs 2.6 and 5.2), the *bvcA* gene comprised a larger proportion of the total RDase genes (27%–53%) in the aqueous phase at locations where TCE and *cis*-DCE were present (downgradient from lenses at Ports 2A, 2B, 2C, 3A, 3C, 4C, and 4D) and near the influent (ports 1B and 1E). At the conclusion of the experiment, when only ethene was detected, the *bvcA* gene abundance was relatively uniform (avg. $1.1 \times 10^7 \pm 5.6 \times 10^6$ copies/mL) comprising 6%–22% of the total aqueous phase RDase genes. In biomass collected from the solid phase, *bvcA* made up a greater proportion of the RDase genes detected in the clay layer (47%–83%), along the top and downgradient edges of the Commerce Street (94–96%) and F-95 sand lenses (44%–73%), and on the downgradient edge of the Appling soil lens (32%), locations that served as an ongoing source of chlorinated ethenes. Similar to the *vcrA gene,* cells harboring the *bvcA gene* were primarily associated with the aqueous phase (93%–100%). The 16S rRNA and RDase gene copies contained in each sample are included as Table SM-1. Overall, the abundance of RDase genes exceeded the abundance of *Dhc* 16S rRNA genes by an average of 3.64-fold ±5.61, which is consistent with previous studies (Cápiro et al., 2015; Damgaard et al., 2013b;

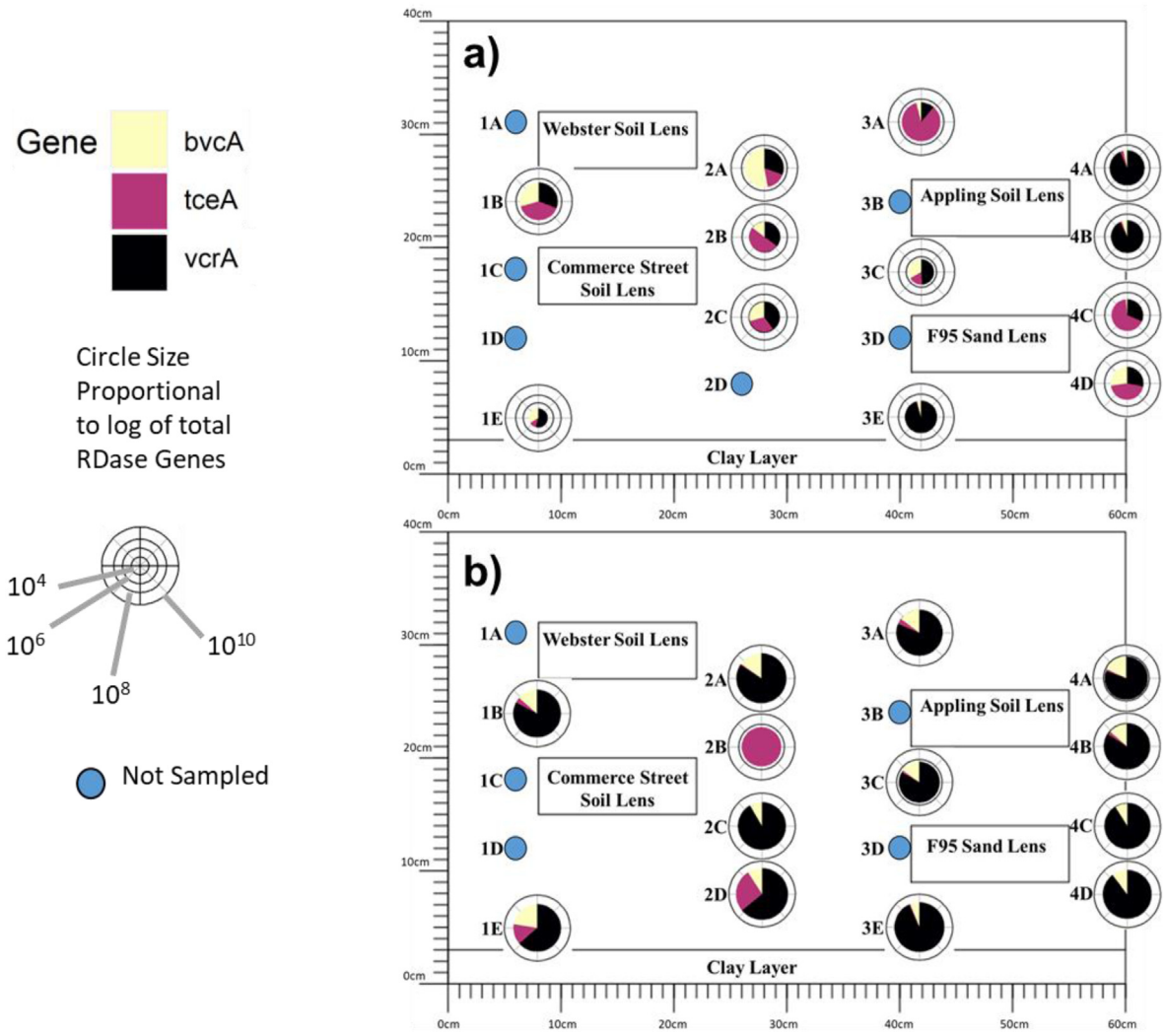

Fig. 4. Aqueous RDase gene abundance and composition (a) 2.6 PVs (8 days) following bioaugmentation and (b) final aqueous samples, 9.8 PVs (37 days) following bioaugmentation.

Van Der Zaan et al., 2010).

The spatial variation in the proportion of cells harboring each RDase gene is a result of the physical properties of the lens materials and their effect on the mass transfer of electron acceptors (i.e., chlorinated ethenes). The Webster and F-95 lenses had the lowest hydraulic conductivity, which impeded the flushing of TCE from these lenses and resulted in longer exposure of cells to TCE and *cis*-DCE, thus favoring cells harboring the *tceA* and *bvcA* genes (Liang et al., 2015; Walker et al., 2005). Although Appling soil has a hydraulic conductivity equal to the Commerce Street material (Table 2), its position further downgradient from the influent chamber facilitated rapid TCE flushing during biotic treatment as TCE daughter products were measured in nearby ports, thereby increasing the TCE concentration gradient between the lens and the surrounding background material. This rapid flushing of TCE favored *Dhc* cells harboring the *vcrA* gene (87%). The overall abundance of RDase genes was approximately one order-of-magnitude lower in the clay, $1.6 \times 10^6 \pm 9.1 \times 10^5$ gene copies/mass of porous media containing 1 mL of water, when compared with the background porous media and lenses ($4.6 \times 10^7 \pm 1.29 \times 10^8$ gene copies/mass of porous media containing 1 mL of water). This result is consistent with the low hydraulic conductivity of the clay that limits penetration of the inoculum into the clay and impedes electron donor delivery.

4. Conclusions

The heterogeneous aquifer cell, packed with porous media representing a range of permeabilities and OC content, enabled examination of the influence of heterogeneity on contaminant mass transfer at a higher resolution than would be possible at the field-scale. Here, MRD enhanced back diffusion by 12% over abiotic conditions alone, with local enhancements up to 53% measured where TCE was stored in low-permeability and high-OC lenses, resulting in increased overall mass flux of chlorinated ethenes from the aquifer cell. Future work on modeling of bioremediation performance should incorporate bioenhanced desorption and diffusion to improve the accuracy of predicted cleanup times, especially in formations with high permeability contrasts. In particular, bioenhancement may substantially impact cleanup times in aquifers with thick low-permeability zones or interbedded high- and low-permeability materials. Under such conditions, more detailed modeling will likely reduce predicted cleanup times and may allow bioremediation to be proposed as a remedy in locations where it

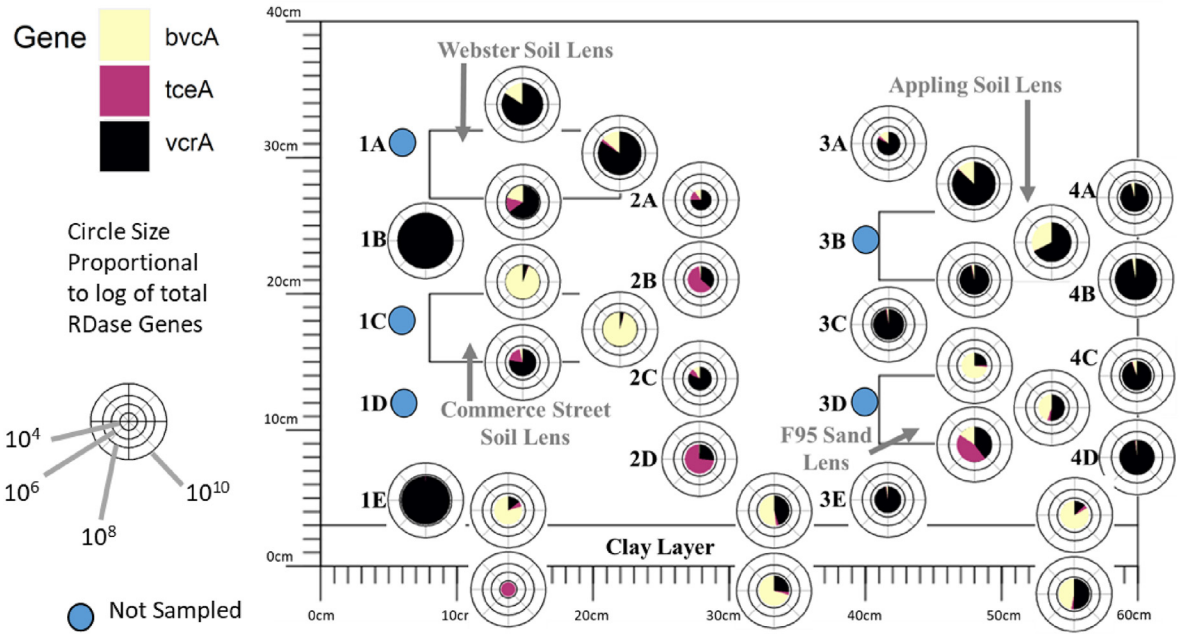

Fig. 5. RDase gene abundance and composition in soil samples at end of experiment, 9.8 PVs (37 days) following bioaugmentation.

was previously thought to be inefficient or infeasible.

Subsurface heterogeneity represented in the aquifer cell resulted in variations in the availability of electron acceptor, shifting the *Dhc* strains present from cells harboring the *tceA* gene in locations where TCE was available to cells harboring the *vcrA* gene where VC was available. Cells harboring the *bvcA* gene were most abundant near low-permeability, high OC materials where *cis*-DCE was available due to the preferential utilization of this electron acceptor. The observed shift in the predominant *Dhc* strain with changes in electron acceptor abundance demonstrates the importance of maintaining a robust dechlorinating community harboring multiple RDase genes and monitoring multiple strains to obtain more complete information for the assessment of bioremediation progress. If the necessary strains are present, the dechlorinating microbial population (e.g., *Geo* and *Dhc* strains) adapts to changes in electron acceptor availability caused by the transport of chlorinated ethenes into and out of low-permeability and highly sorptive soils. Such shifts in the microbial population allow efficient transformation of chlorinated ethenes to ethene over the course of a bioremediation application.

The detailed experimental and mathematical modeling assessment of bioaugmentation and biostimulation in the heterogeneous aquifer cell revealed that:

- Differences in hydraulic conductivity and OC content controlled desorption and back diffusion of sequestered chlorinated solvents from OC and low-permeability zones.
- Organohalide respiring bacteria enhance the mass transfer of TCE out of the low-permeability regions over abiotic diffusion processes alone.
- The greatest bioenhancement of back diffusion occurred in regions of contrasting hydraulic conductivity and organic carbon content.
- Model simulations accounting for heterogeneity in physical and chemical properties quantified local bioenhancement of back diffusion up to 53%
- *Dhc* cells were capable of penetrating low-permeability porous media including clays, contributing to enhanced back diffusion.
- The distribution of specific *Dhc* strains was influenced by the availability of electron acceptors within and near soils of differing physical properties.

Declaration of competing interest

The authors declare that they have no known competing financial interests or personal relationships that could have appeared to influence the work reported in this paper.

CRediT authorship contribution statement

Jason P. Hnatko: Investigation, Methodology, Visualization, Writing - original draft. **Lurong Yang:** Software, Investigation, Visualization, Methodology, Writing - original draft. **Kurt D. Pennell:** Conceptualization, Funding acquisition, Writing - review & editing. **Linda M. Abriola:** Conceptualization, Validation, Funding acquisition, Writing - review & editing. **Natalie L. Cápiro:** Conceptualization, Supervision, Funding acquisition, Writing - review & editing.

Acknowledgements

Funding for this research was provided by the Strategic Environmental Research and Development Program (SERDP) under Contract W912HQ-13-C-0011, Project ER-2311: Development of an Integrated Field Test/Modeling Protocol for Efficient *In Situ* Bioremediation Design and Performance Uncertainty Assessment. The authors thank Samuel Gaeth, Jessica Cooper, and Tian Tang for their assistance with sampling and data analysis, and SiREM for providing the KB-1® culture used in the aquifer cell experiment. The contents of this manuscript have not been subject to agency review and do not necessarily represent the views of the sponsoring agency.

Appendix A. Supplementary data

Supplementary data to this article can be found online at https://doi.org/10.1016/j.chemosphere.2020.126842.

References

Adrian, L., Löffler, F.E., Field, J.a., Dolfng, J., McCarty, P.L., Atashgahi, S., Lu, Y., Smidt, H., Zinder, S.H., Moe, W.M., Rainey, F.a., Yan, J., Maillard, J., Holliger, C., Futagami, T., Furukawa, K., Goris, T., Diekert, G., Sanford, R.a., Chowdhary, J., Mayer-Blackwell, K., Sewell, H., Fincker, M., Spormann, A.M., Wei, K., Grostern, A., Chan, W.W.M., Richardson, R.E., Edwards, E.a., Kruse, T., Lechner, U., Hug, L.a., Schubert, T., Renpenning, J., Nijenhuis, I., Moore, T.C., Escalante-Semerena, J.C., Dobbek, H., Leys, D., Aulenta, F., Rossetti, S., Matturro, B., Tandoi, V., Verdini, R., Majone, M., Steffan, R.J., Schaefer, C.E., He, J., Bedard, D.L., May, H.D., Sowers, K.R., Hunkeler, D., 2016. Organohalide-Respiring Bacteria. https://doi.org/10.1007/978-3-662-49875-0.

Amos, B.K., Suchomel, E.J., Pennell, K.D., Löffler, F.E., 2009. Spatial and temporal distributions of Geobacter lovleyi and Dehalococcoides spp. during bio-enhanced PCE-NAPL dissolution. Environ. Sci. Technol. 43, 1977–1985. https://doi.org/10.1021/es8027692.

Amos, B.K., Ritalahti, K.M., Cruz-Garcia, C., Padilla-Crespo, E., Löffler, F.E., 2008. Oxygen effect on Dehalococcoides viability and biomarker quantification. Environ. Sci. Technol. 42, 5718–5726. https://doi.org/10.1021/es703227g.

Baldwin, B.R., Taggart, D., Chai, Y., Wandor, D., Biernacki, A., Sublette, K.L., Wilson, J.T., Walecka-Hutchison, C., Coladonato, C., Goodwin, B., 2017. Bioremediation management reduces mass discharge at a chlorinated DNAPL site. Groundw. Monit. Remediat. 37, 58–70. https://doi.org/10.1111/gwmr.12211.

Ball, W.P., Liu, C., Xia, G., Young, D.F., 1997. A diffusion-based interpretation of tetrachloroethene and trichloroethene concentration profiles in a groundwater aquitard. Water Resour. Res. 33, 2741–2757. https://doi.org/10.1029/97WR02135.

Behrens, S., Azizian, M.F., McMurdie, P.J., Sabalowsky, A., Dolan, M.E., Semprini, L., Spormann, A.M., 2008. Monitoring abundance and expression of "Dehalococcoides" species chloroethene-reductive dehalogenases in a tetrachloroethene-dechlorinating flow column. Appl. Environ. Microbiol. 74, 5695–5703. https://doi.org/10.1128/AEM.00926-08.

Cápiro, N.L., Löffler, F.E., Pennell, K.D., 2015. Spatial and temporal dynamics of organohalide-respiring bacteria in a heterogeneous PCE-DNAPL source zone. J. Contam. Hydrol. 182, 78–90. https://doi.org/10.1016/j.jconhyd.2015.08.007.

Cápiro, N.L., Wang, Y., Hatt, J.K., Lebron, C., Pennell, K.D., Löffler, F.E., 2014. Distribution of organohalide-respiring bacteria between solid and aqueous phases. Environ. Sci. Technol. 48, 10878–10887. https://doi.org/10.1021/es501320h.

Chambon, J.C., Broholm, M.M., Binning, P.J., Bjerg, P.L., 2010. Modeling multicomponent transport and enhanced anaerobic dechlorination processes in a single fracture-clay matrix system. J. Contam. Hydrol. 112, 77–90. https://doi.org/10.1016/j.jconhyd.2009.10.008.

Chapman, S.W., Parker, B.L., Sale, T.C., Doner, L.A., 2012. Testing high resolution numerical models for analysis of contaminant storage and release from low permeability zones. J. Contam. Hydrol. 106–116. https://doi.org/10.1016/j.jconhyd.2012.04.006, 136–137.

Chapman, S.W., Parker, B.L., 2005. Plume persistence due to aquitard back diffusion following dense nonaqueous phase liquid source removal or isolation. Water Resour. Res. 41, 1–16. https://doi.org/10.1029/2005WR004224.

Chen, M., Abriola, L.M., Amos, B.K., Suchomel, E.J., Pennell, K.D., Löffler, F.E., Christ, J.A., 2013. Microbially enhanced dissolution and reductive dechlorination of PCE by a mixed culture: model validation and sensitivity analysis. J. Contam. Hydrol. 151, 117–130. https://doi.org/10.1016/j.jconhyd.2013.05.005.

Chen, L., Miller, G.A., Kibbey, T.C.G., 2007. Rapid pseudo-static measurement of hysteretic capillary pressure-saturation relationships in unconsolidated porous media. Geotech. Test J. 30, 474–483. https://doi.org/10.1520/GTJ100850.

Clark, K., Taggart, D.M., Baldwin, B.R., Ritalahti, K.M., Murdoch, R.W., Hatt, J.K., Lo, F.E., 2018. Normalized Quantitative PCR Measurements as Predictors for Ethene Formation at Sites Impacted with Chlorinated Ethenes. https://doi.org/10.1021/acs.est.8b04373.

Damgaard, I., Bjerg, P.L., Jacobsen, C.S., Tsitonaki, A., Kerrn-Jespersen, H., Broholm, M.M., 2013a. Performance of full-scale enhanced reductive dechlorination in clay till. Ground water monit. Remediat 33, 48–61. https://doi.org/10.1111/j1745-6592.2012.01405.x.

Damgaard, I., Bjerg, P.L., Bælum, J., Scheutz, C., Hunkeler, D., Jacobsen, C.S., Tuxen, N., Broholm, M.M., 2013b. Identification of chlorinated solvents degradation zones in clay till by high resolution chemical, microbial and compound specific isotope analysis. J. Contam. Hydrol. 146, 37–50. https://doi.org/10.1016/j.jconhyd.2012.11.010.

Doğan-Subaşi, E., Bastiaens, L., Leys, N., Boon, N., Dejonghe, W., 2014. Quantitative and functional dynamics of Dehalococcoides spp. and its tceA and vcrA genes under TCE exposure. Biodegradation 25, 493–504. https://doi.org/10.1007/s10532-013-9676-8.

Duhamel, M., Edwards, E.A., 2007. Growth and yields of dechlorinators, acetogens, and methanogens during reductive dechlorination of chlorinated ethenes and dihaloelimination of 1,2-dichloroethane. Environ. Sci. Technol. 41, 2303–2310. https://doi.org/10.1021/es062010r.

Duhamel, M., Mo, K., Edwards, E. a, 2004. Characterization of a highly enriched Dehalococcoides -containing culture that grows on vinyl chloride and. Appl. Environ. Microbiol. 70, 5538–5545. https://doi.org/10.1128/AEM.70.9.5538.

Duhamel, M., Wehr, S.D., Yu, L., Rizvi, H., Seepersad, D., Dworatzek, S., Cox, E.E., Edwards, E.a., 2002. Comparison of anaerobic dechlorinating enrichment cultures maintained on tetrachloroethene, trichloroethene, cis-dichloroethene and vinyl chloride. Water Res. 36, 4193–4202. https://doi.org/10.1016/S0043-1354(02)00151-3.

Gaeth, S.P., 2017. Examining Reactive Minerals, Sulfide, and Bioremediation Interactions for Improved Chlorinated Solvent Detoxification. Tufts University.

Grostern, A., Edwards, E.A., 2006. Growth of Dehalobacter and Dehalococcoides spp. during degradation of chlorinated ethanes. Appl. Environ. Microbiol. 72, 428–436. https://doi.org/10.1128/AEM.72.1.428-436.2006.

He, J., Sung, Y., Krajmalnik-Brown, R., Ritalahti, K.M., Löffler, F.E., 2005. Isolation and characterization of Dehalococcoides sp. strain FL2, a trichloroethene (TCE)- and 1,2-dichloroethene-respiring anaerobe. Environ. Microbiol. 7, 1442–1450. https://doi.org/10.1111/j.1462-2920.2005.00830.x.

He, J., Ritalahti, K.M., Aiello, M.R., Löffler, F.E., 2003. Complete detoxification of vinyl chloride by an anaerobic enrichment culture and identification of the reductively dechlorinating population as a Dehalococcoides species. Appl. Environ. Microbiol. 69, 996–1003. https://doi.org/10.1128/AEM.69.2.996-1003.2003.

Hood, E.D., Major, D.W., Quinn, J.W., Yoon, W.S., Gavaskar, A., Edwards, E.A., 2008. Demonstration of enhanced bioremediation in a TCE source area at launch complex 34, cape canaveral air force station. Ground Water Monit. Remed. 28, 98–107. https://doi.org/10.1111/j.1745-6592.2008.00197.x.

Johnson, R.L., Cherry, J.A., Pankow, J.F., 1989. Diffusive contaminant transport in natural clay: a field example and implications for clay-lined waste disposal sites. Environ. Sci. Technol. 23, 340–349. https://doi.org/10.1021/es00180a012.

Joo, J.C., Shackelford, C.D., Reardon, K.F., 2008. Association of humic acid with metal (hydr)oxide-coated sands at solid-water interfaces. J. Colloid Interface Sci. 317, 424–433. https://doi.org/10.1016/j.jcis.2007.09.061.

Kielhorn, J., Melber, C., Wahnschaffe, U., Aitio, a, Mangelsdorf, I., 2000. Vinyl chloride: still a cause for concern. Environ. Health Perspect. 108, 579–588. https://doi.org/10.2307/3434875.

Lee, P.K.H., Macbeth, T.W., Sorenson, K.S., Deeb, R.a., Alvarez-Cohen, L., 2008. Quantifying genes and transcripts to assess the in situ physiology of "Dehalococcoides" spp. in a trichloroethene-contaminated groundwater site. Appl. Environ. Microbiol. 74, 2728–2739. https://doi.org/10.1128/AEM.02199-07.

Lendvay, J.M., Löffler, F.E., Dollhopf, M., Aiello, M.R., Daniels, G., Fathepure, B.Z., Gebhard, M., Heine, R., Helton, R., Shi, J., Krajmalnik-Brown, R., Major, C.L., Barcelona, M.J., Petrovskis, E., Hickey, R., Tiedje, J.M., Adriaens, P., 2003. Bioreactive barriers: a comparison of bioaugmentation and biostimulation for chlorinated solvent remediation. Environ. Sci. Technol. 37, 1422–1431. https://doi.org/10.1021/es025985u.

Li, Y.-H., Gregory, S., 1974. Diffusion of ions in sea water and in deep-sea sediments. Geochem. Cosmochim. Acta 38, 703–714. https://doi.org/10.1016/0016-7037(74)90145-8.

Liang, X., Molenda, O., Tang, S., Edwards, E.a., 2015. Identity and substrate specificity of reductive dehalogenases expressed in Dehalococcoides-containing enrichment cultures maintained on different chlorinated ethenes. Appl. Environ. Microbiol. 81, 4626–4633. https://doi.org/10.1128/AEM.00536-15.

Lima, G. da P., Sleep, B.E., 2007. The spatial distribution of eubacteria and archaea in sand-clay columns degrading carbon tetrachloride and methanol. J. Contam. Hydrol. 94, 34–48. https://doi.org/10.1016/j.jconhyd.2007.05.001.

Loffler, F.E., Ritalahti, K.M., Zinder, S.H., 2013. Dehalococcoides and reductive dechlorination of chlorinated solvents. In: Stroo, H.F., Leeson, A., Ward, C.H. (Eds.), Bioaugmentation for Groundwater Remediation. Springer, New York, NY, pp. 39–88.

Löffler, F.E., Yan, J., Ritalahti, K.M., Adrian, L., Edwards, E.A., Konstantinidis, K.T., Müller, J.A., Fullerton, H., Zinder, S.H., Spormann, A.M., 2013. Dehalococcoides mccartyi gen. nov., sp. nov., obligately organohalide-respiring anaerobic bacteria relevant to halogen cycling and bioremediation, belong to a novel bacterial class, Dehalococcoidia classis nov., order Dehalococcoidales ord. nov. and famil. Int. J. Syst. Evol. Microbiol. 63, 625–635. https://doi.org/10.1099/ijs.0.034926-0.

Löffler, F.E., Sanford, R.A., Ritalahti, K.M., 2005. Enrichment, cultivation, and detection of reductively dechlorinating bacteria. Methods Enzymol. 397, 77–111. https://doi.org/10.1016/S0076-6879(05)97005-5.

Major, D.W., McMaster, M.L., Cox, E.E., Edwards, E.a., Dworatzek, S.M., Hendrickson, E.R., Starr, M.G., Payne, J.A., Buonamici, L.W., 2002. Field demonstration of successful bioaugmentation to achieve dechlorination of tetrachloroethene to ethene. Environ. Sci. Technol. 36, 5106–5116. https://doi.org/10.1021/es0255711.

Marcet, T.F., Cápiro, N.L., Yang, Y., Löffler, F.E., Pennell, K.D., 2018a. Impacts of low-temperature thermal treatment on microbial detoxification of tetrachloroethene under continuous flow conditions. Water Res. 145, 21–29. https://doi.org/10.1016/j.watres.2018.07.076.

Marcet, T.F., Cápiro, N.L., Morris, L.A., Hassan, S.M., Yang, Y., Löffler, F.E., Pennell, K.D., 2018b. Release of electron donors during thermal treatment of soils. Environ. Sci. Technol. 52, 3642–3651. https://doi.org/10.1021/acs.est.7b06014.

Marcet, T.F., 2014. Secondary Impacts of in Situ Chlorinated Solvent Remediation Due to Metal Sulfide Preceipitation and Thermal Treatment. Tufts University.

Maymó-Gatell, X., Anguish, T., Zinder, S.H., 1999. Reductive dechlorination of chlorinated ethenes and 1, 2-dichloroethane by "Dehalococcoides ethenogenes" 195. Appl. Environ. Microbiol. 65, 3108–3113.

Mccarty, P.L., 2010. Groundwater contamination by chlorinated solvents: history, remediation technologies and strategies. In: Stroo, H.F., Ward, C.H. (Eds.), In Situ

Remediation of Chlorinated Solvent Plumes. Springer, New York, pp. 1–28.
McGuire, T.M., McDade, J.M., Newell, C.J., 2006. Performance of DNAPL source depletion technologies at 59 chlorinated solvent-impacted sites. Ground Water Monit. Remed. 26, 73–84. https://doi.org/10.1111/j.1745-6592.2006.00054.x.
Mirza, B.S., Sorensen, D.L., Dupont, R.R., McLean, J.E., 2016. Dehalococcoides abundance and alternate electron acceptor effects on large, flow-through trichloroethene dechlorinating columns. Appl. Microbiol. Biotechnol. 100, 2367–2379. https://doi.org/10.1007/s00253-015-7112-1.
Pankow, J.F., Feenstra, S., Cherry, J.A., Ryan, M.C., 1996. Dense chlorinated solvents and other DNAPLs in groundwater : background and history of the problem. In: Pankow, J.F., Cherry, J.A. (Eds.), Dense Chlorinated Solvents and Other DNAPLs in Groundwater. Waterloo Press, Guelph, Ontario, Canada, pp. 1–52.
Parker, B.L., Chapman, S.W., Guilbeault, M.A., 2008. Plume persistence caused by back diffusion from thin clay layers in a sand aquifer following TCE source-zone hydraulic isolation. J. Contam. Hydrol. 102, 86–104. https://doi.org/10.1016/j.jconhyd.2008.07.003.
Pennell, K.D., Boyd, S. a, Abriola, L.M., 1995. Surface area of soil organic matter reexamined. Soil Sci. Soc. Am. J. 59, 1012–1018. https://doi.org/10.2136/sssaj1995.03615995005900040008x.
Ritalahti, K.M., Amos, B.K., Sung, Y., Wu, Q., Koenigsberg, S.S., Löffler, F.E., 2006. Quantitative PCR targeting 16S rRNA and reductive dehalogenase genes simultaneously monitors multiple Dehalococcoides strains. Appl. Environ. Microbiol. 72, 2765–2774. https://doi.org/10.1128/AEM.72.4.2765-2774.2006.
Rodriguez, D., 2006. Significance of diffused zone mass storage and rebound in determing the longevity of solute plumes emanating from heterogeneous DNAPL source zones. PhD Thesis. https://doi.org/10.1073/pnas.0703993104.
Sale, T., Parker, B.L., Newell, C.J., Devlin, J.F., 2013. Management of Contaminants Stored in Low Permeability Zones. SERDP Project ER-1740.
Schaefer, C.E., Towne, R.M., Vainberg, S., McCray, J.E., Steffan, R.J., 2010. Bioaugmentation for treatment of dense non-aqueous phase liquid in fractured sandstone blocks. Environ. Sci. Technol. 44, 4958–4964. https://doi.org/10.1021/es1002428.
Scheutz, C., Broholm, M.M., Durant, N.D., Weeth, E.B., Jorgensen, T.H., Dennis, P., Jacobsen, C.S., Cox, E.E., Chambon, J.C., Bjerg, P.L., 2010. Field evaluation of biological enhanced reductive dechlorination of chloroethenes in clayey till. Environ. Sci. Technol. 44, 5134–5141. https://doi.org/10.1021/es1003044.
Simpkin, T.J., Norris, R.D., 2010. Engineering and implementation challenges for chlorinated solvent remediation. In: Stroo, H.F., Ward, C.H. (Eds.), In Situ Remediation of Chlorinated Solvent Plumes1. Springer, New York, pp. 109–143.
Sleep, B.E., Seepersad, D.J., Mo, K., Heidorn, C.M., Hrapovic, L., Morrill, P.L., McMaster, M.L., Hood, E.D., Lebron, C., Lollar, B.S., Major, D.W., Edwards, E.A., 2006. Biological enhancement of tetrachloroethene dissolution and associated microbial community changes. Environ. Sci. Technol. 40, 3623–3633. https://doi.org/10.1021/es051493g.
Suchomel, E.J., Ramsburg, C.A., Pennell, K.D., 2007. Evaluation of trichloroethene recovery processes in heterogeneous aquifer cells flushed with biodegradable surfactants. J. Contam. Hydrol. 94, 195–214. https://doi.org/10.1016/j.jconhyd.2007.05.011.
Sung, Y., Fletcher, K.E., Ritalahti, K.M., Apkarian, R.P., Ramos-Hernandez, N., Sanford, R. a, Mesbah, N.M., Loffler, F.E., 2006. Geobacter lovleyi sp. nov. Strain SZ, a novel metal-reducing and tetrachloroethene-dechlorinating bacterium. Appl. Environ. Microbiol. 72, 2775–2782. https://doi.org/10.1128/AEM.72.4.2775-2782.2006.
Taylor, T.P., Pennell, K.D., Abriola, L.M., Dane, J.H., 2001. Surfactant enhanced recovery of tetrachloroethylene from a porous medium containing low permeability lenses. J. Contam. Hydrol. 48, 325–350. https://doi.org/10.1016/S0169-7722(00)00185-6.
Tillotson, J.M., Borden, R.C., 2017. Rate and extent of chlorinated ethene removal at 37 ERD sites. J. Environ. Eng. 143, 1–10. https://doi.org/10.1061/(ASCE)EE.1943-7870.0001224.
Van Der Zaan, B., Hannes, F., Hoekstra, N., Rijnaarts, H., De Vos, W.M., Smidt, H., Gerritse, J., 2010. Correlation of Dehalococcoides 16S rRNA and chloroethene-reductive dehalogenase genes with geochemical conditions in chloroethene-contaminated groundwater. Appl. Environ. Microbiol. 76, 843–850. https://doi.org/10.1128/AEM.01482-09.
van Genuchten, M.T., Alves, W.J., 1982. Analytical Solutions of the One-Dimensional Convective-Dispersive Solute Transport Equation (No. 157268), Technical Bulletins. United States Department of Agriculture, Economic Research Service.
Verschueren, K., 2001. Handbook of Environmental Data on Organic Chemicals. Wiley.
Walker, S.L., Redman, J.a., Elimelech, M., 2005. Influence of growth phase on bacterial deposition: interaction mechanisms in packed-bed column and radial stagnation point flow systems. Environ. Sci. Technol. 39, 6405–6411. https://doi.org/10.1021/es050077t.
Yang, Y., McCarty, P.L., 2000. Biologically enhanced dissolution of tetrachloroethene DNAPL. Environ. Sci. Technol. 34, 2979–2984. https://doi.org/10.1021/es991410u.
Yang, L., Wang, X., Mendoza-Sanchez, I., Abriola, L.M., 2018. Modeling the influence of coupled mass transfer processes on mass flux downgradient of heterogeneous DNAPL source zones. J. Contam. Hydrol. 211, 1–14. https://doi.org/10.1016/j.jconhyd.2018.02.003.
Yang, Y., Cápiro, N.L., Yan, J., Marcet, T.F., Pennell, K.D., Löffler, F.E., 2017. Resilience and recovery of Dehalococcoides mccartyi following low pH exposure. FEMS Microbiol. Ecol. 93, 1–9. https://doi.org/10.1093/femsec/fix130.
Yoshikawa, M., Takeuchi, M., Zhang, M., 2017. Distribution of Dehalococcoides 16S rRNA and dehalogenase genes in contaminated sites. Environ. Nat. Resour. Res. 7, 37. https://doi.org/10.5539/enrr.v7n2p37.